Solar Energy 170 (2018) 95–101

Contents lists available at ScienceDirect

Solar Energy

journal homepage: www.elsevier.com/locate/solener

The study of the defect removal etching of black silicon for diamond wire sawn multi-crystalline silicon solar cells

Guoyu Su[a,b,c], Xiaowan Dai[a], Ke Tao[a], Hengchao Sun[a], Rui Jia[a,*], Zhi Jin[a], Xinyu Liu[a], Hongzhi Liu[d], Shouqiang Liu[d], Chun Xu[e], Yujia Cao[e], Yan Zhao[e], Hui Qu[e], Bin Liu[e], Bihua Chen[e]

[a] Institute of Microelectronics, Chinese Academy of Sciences, 3# Bei-Tu-Cheng West Road, Beijing 100029, China
[b] Jiangsu R&D Center for Internet of Things, 200# Ling-Hu Avenue, Jiangsu 214028, China
[c] University of Chinese Academy of Sciences, Beijing 100049, China
[d] Beijing Zhongkexin Electronics Equipment Co., Ltd, Beijing, China
[e] Jiangsu Shunfeng Photovoltaic Technology CO., LTD, Jiangsu, China

ARTICLE INFO

Keywords:
Multi-crystalline silicon solar cell
Diamond wire sawing
Defect removal etching
Metal-assisted chemical etching

ABSTRACT

We produced low-reflectivity nanostructured black silicon by metal-assisted chemical etching (MACE) technology on the 15.6 cm × 15.6 cm diamond wire sawn (DWS) multi-crystalline silicon (mc-Si) wafers. Subsequently, defect removal etching (DRE) processes were carried out for various times to form nanohills with different sizes on the wafer surface. The experimental results indicated that the DRE process could influence the size of the nanohills, reflectivity and the recombination velocities of the silicon wafers. It was found that for the black silicon wafer, with the increasing of DRE time, the reflectivity became larger and the passivation effect became better. The reflectivity and the passivation effect can be adjusted by suitable DRE processes. By this way, we successfully fabricated the DWS mc-Si solar cell (15.6 cm × 15.6 cm) with the highest conversion efficiency of 19.07%, showing an improvement in efficiency of 0.6% compared to a DWS mc-Si solar cell (15.6 cm × 15.6 cm) prepared by conventional acidic texturization.

1. Introduction

In recent years, crystalline silicon wafers have remained the most widely used materials in the photovoltaic (PV) market due to higher efficiencies and lower cost (Yu et al., 2016). Generally, the cost of multi-crystalline silicon (mc-Si) wafers is lower than that of Czochralski (CZ) mono-crystalline wafers, and the mc-Si solar cell has the larger PV market share (Yu et al., 2017; Huang et al., 2017). In recent years, diamond wire sawn (DWS) mc-Si wafers have become a hot spot in the PV market due to its lower cost than slurry wire sawn (SWS) mc-Si (Xiao et al., 2016; Kim et al., 2016; Liu et al., 2017; Holt et al., 2010). However, there is no cost-effective way to texture the DWS mc-Si wafer, and there is a big problem for DWS mc-Si to improve the conversion efficiency by greatly decreasing the reflectivity (Meinel et al., 2012; Meinel et al., 2014; Sopori et al., 2015). Thus the black silicon technologies were proposed to solve this problem (Wehrspohn and Sprafke, 2014).

Black silicon with extremely low reflectivity is due to the fact that its surface is covered with a layer of nano-sized or micro-sized structures, which effectively enhance the absorption of light. As a consequence, the silicon wafers appear black so called “black silicon” (Liu et al., 2014). Black silicon fabrication techniques include reactive ion etching (RIE), femtosecond laser technique, metal-assisted chemical etching (MACE) and electrochemical etching (Wehrspohn and Sprafke, 2014). RIE and MACE techniques were regarded as the cost-effective ways to texture crystalline silicon wafer and the next-generation texture technologies (Park et al., 2013; Kim et al., 2015; Jiang et al., 2017; Yang et al., 2017). In fact, the MACE technique had lower cost than the RIE technique because of the using of a wet chemical process (Huang et al., 2011). For MACE, Au and Ag are the two most popular metal candidates. Koynov et al. used Au metal to produce a black silicon surface with extremely low reflectivity (Koynov et al., 2006). Solar cells fabricated using this technique showed a remarkable increasing of short-circuit current density (Koynov et al., 2007). Niu et al. successfully textured DWS mc-Si wafers by Ag-assisted etching combined with an auxiliary etching (Niu et al., 2016). Su et al. fabricated 18.31%-efficient DWS mc-Si solar cells by using Ag-assisted chemical etching on an industrial production line (Cao et al., 2015).

Although black silicon with an extremely low reflectivity can be fabricated using the MACE technique, the performances of black-

* Corresponding author.
E-mail address: imesolar@126.com (R. Jia).

https://doi.org/10.1016/j.solener.2018.04.066
Received 26 December 2017; Received in revised form 6 April 2018; Accepted 30 April 2018
Available online 19 May 2018
0038-092X/

silicon-based solar cells are unsatisfactory. Actually, the defect removal etching (DRE) process strongly affects black silicon solar cells (Xiao et al., 2014). Su et al. prepared black mc-Si solar cells using the MACE process followed by etching in NaOH/H_2O solution for the DRE process. The highest efficiency obtained for black mc-Si solar cells prepared with and without the DRE process is 18.45% and 16.51%, respectively (Ye et al., 2015). Kumagai also demonstrated that the DRE process (HNO_3/HF/H_2O and NaOH) influences the efficiency of DWS mc-Si solar cells (Kumagai, 2015). There is still no detail report about the effect of DRE process time on the reflectivity and passivation effect of black silicon wafers.

In this work, black DWS mc-Si wafers were fabricated using a MACE and DRE processes. The DRE process includes using a HNO_3/HF/H_2O_2/H_2O solution etching and a KOH solution etching. Here, we added H_2O_2 into the HNO_3/HF/H_2O solution for slowing and controlling the etching rate of HNO_3/HF/H_2O solution. We also studied the influences of the DRE processing time on the reflectivity, the effect of passivation and the solar cell efficiency. A DWS mc-Si solar cell conversion efficiency of 19.07% was achieved due to the combination of MACE and suitable DRE processes, corresponding to a 0.6% efficiency improvement as opposed to the conventional acidic textured DWS mc-Si.

2. Experimental

DWS mc-Si wafers and SWS mc-Si wafers (15.6 cm × 15.6 cm, 200 ± 10 μm thick, p-type, specific resistivity of 1–3 Ω·cm) were provided by the GCL Company in China. The fabrication procedures used for the black mc-Si solar cells are shown in Fig. 1. First, the saw damage removal (SDR) processes were carried out in a nitric acid/hydrofluoric acid HNO_3/HF/H_2O solution and in a 3% KOH solution, which is the conventional Industry texture method. Black silicon was then fabricated using the MACE process. By the processes, the micron-sized texture were formed on the DWS mc-Si surface. Then the MACE process was performed to form the black silicon on the DWS mc-Si surface with micron-sized textures. First, Ag nanoparticles in $AgNO_3$/HF/H_2O solution were deposited onto the DWS silicon wafers, which were then etched in H_2O_2/HF/H_2O solution to form black silicon structures. Next, wafers were dipped into 70% HNO_3 solution to remove Ag nanoparticles. Subsequently, DRE processes were performed: wafers were

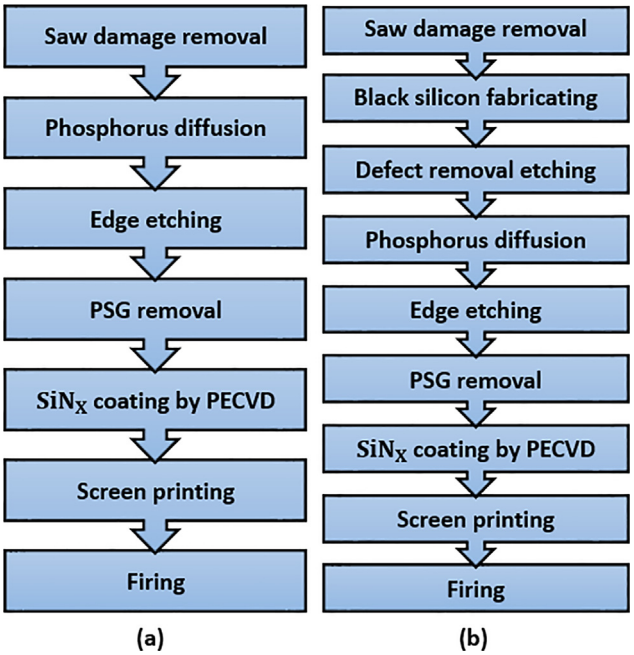

Fig. 1. Fabrication process for (a) traditional acid textured DWS mc-Si solar cells; (b) DWS multi-crystalline black silicon solar cells.

Table 1
Conditions for the acidic DRE processes.

Conditions	Black silicon or not	Ratio of HNO_3 + HF + H_2O_2 + H_2O in DRE	Etching time
C1	No black silicon	–	–
C2	Black silicon	–	–
C3	Black silicon	15:3:1:20	1 min
C4	Black silicon	15:3:1:20	3 min
C5	Black silicon	15:3:1:20	6 min
C6	Black silicon	15:3:0:20	1 min

etched in a HNO_3/HF/H_2O_2/H_2O solution and in a KOH solution for different times to remove surface defects. The conditions for the acidic DRE processes were shown in Table 1 with the KOH solution etching time being kept constant for all samples. Finally, all textured DWS mc-Si wafers underwent the same standard solar cell processing, including phosphorus doping, edge etching for removing the edge, back pn junctions and phosphosilicate glass (PSG) layer, plasma-enhanced chemical vapor deposition (PECVD) of the SiN_x antireflective film, screen printing and sintering of the front and back electrodes.

Structures on the DWS *mc*-Si wafers were investigated by scanning electron microscope (SEM, Hitachi, S-4800, Japan). The reflectance, internal quantum efficiency (IQE) and external quantum efficiency (EQE) were evaluated by measurement of the incident photon to charge carrier efficiency (IPCE) using a solar cell measurement system (sofn, 7-SCSpecII, China). The minority carrier lifetime and I-V curves for cells were measured using a Sinton wafer lifetime tester (Sinton, WCT-120, USA) and an I-V measurement system (QuickSun, 120CA-HC, Finland), respectively. Electroluminescence (EL) images were collected by an EL sorting machine (Zhewei, SA-220, China).

3. Results and discussion

Fig. 2 showed the structures on DWS and SWS mc-Si wafers after the same conventional acidic texture processes. It could be found that the surface of the SWS mc-Si wafer was randomly covered with intensive “worm-like” structures and the DWS mc-Si wafer was only covered with “worm-like” structures along the sawn line traces. The differences between the two samples were caused by the different sawing methods, which led to different damage layers and textured structures on the silicon wafers (Cao et al., 2015). Fig. 3 showed reflectance curves for DWS and SWS mc-Si wafers after conventional acid-textured processes, and Table 2 showed the performances of DWS and SWS mc-Si solar cells. We calculated the weighted average values of the reflectivity under AM1.5 standard conditions over the wavelength range from 300 to 1100 nm. The weighted average reflectance value is defined as

$$R_a = \frac{\int_{300}^{1100} R(\lambda)N(\lambda)d\lambda}{\int_{300}^{1100} N(\lambda)d\lambda} \quad (1)$$

where $R(\lambda)$ is the total reflectance and $N(\lambda)$ is the solar flux under AM1.5 standard conditions (Menna et al., 1995). The weighted average reflectance values for the acid-textured SWS structure with and without SiN_x film were 31.12% and 12.10%, respectively. For comparison, the weighted average reflectance values for the acid-textured DWS structure with and without SiN_x film were 36.39% and 13.49%, respectively. We could see that these values of DWS mc-Si wafers were higher than those of SWS wafers, leading to a lower short-circuit current density J_{sc} for the DWS mc-Si solar cell. On the basis of our preliminary work, the efficiency of an acid-textured DWS mc-Si solar cell was normally 0.14% lower than that of the SWS solar cell, which was mainly caused by the higher light reflection of DWS mc-Si wafer. Hence, according to the above results, the conventional acidic texture method is unsuitable for the DWS mc-Si solar cell.

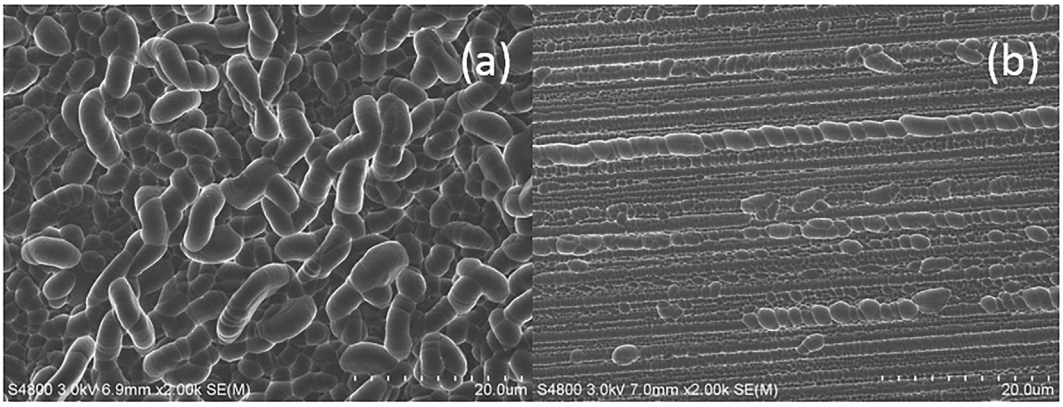

Fig. 2. SEM of images on the silicon wafers surface after the same conventional acidic texture processes. The surfaces were covered by micron-sized textures with different distribution (a) SWS mc-Si wafers; (b) DWS mc-Si wafers.

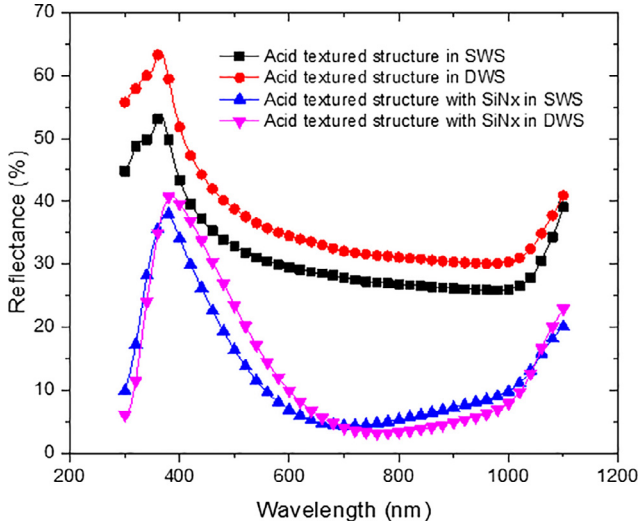

Fig. 3. Reflectance curves for the acid-textured structure on the SWS mc-Si wafer and the DWS mc-Si wafer; reflectance curves for the wafer with SiNx.

Table 2
Performance comparisons of conventional acid textured DWS and SWS mc-Si solar cells.

	V_{oc}/mV	J_{sc}/mA cm^{-2}	R_s/Ω	*FF*/%	Eff./%
SWS	635	36.66	0.0017	79.99	18.61
DWS	636	36.42	0.0020	79.75	18.47

DWS mc-Si wafers with extremely low reflectivity could be obtained by using the MACE technique. However, we found that the conversion efficiency of MACE textured DWS mc-Si solar cell without DRE processes was lower than that of conventional acid-textured DWS mc-Si solar cells with the efficiency of 18.47% due to the strong surface recombination of black silicon. Therefore, DRE processes were needed to remove recombination centers. Fig. 4 showed nanostructures formed with different times on the black silicon surface followed the DRE process. For compassion, the conventional acidic-texture DWS mc-Si sample was shown in Fig. 4(c1). After the SDR processes, many micron-sized irregular pits were observed on the surface, as shown for sample C1. It could be seen from SEM image of sample C2 without DRE processes that the black silicon nanostructures were rough. This image clearly showed the existences of large quantity of surface defects. These defects influenced the effects of phosphorus diffusion and passivation by SiN_x, leading to a reduction of the cell efficiency. Samples C3 to C5 processed using different DRE processing times were covered by nanohills with different sizes, where the size of the nanohills decreases with the increasing etching time. The $HNO_3/HF/H_2O_2/H_2O$ in the DRE process can be explained by two steps. Firstly, the rough black silicon structures were oxidized by HNO_3. Secondly, the silicon oxide was dissolved by HF. Therefore, the rough black silicon structures were etched and modified.

For comparison, the SEM image of sample C6 was shown with the different acid DRE solution, that is $HNO_3/HF/H_2O$ without H_2O_2. Although this sample was processed using the same etching time (1 min) as that of sample C3, the nanostructures for C6 were smoother than those of C3. Actually, black silicon could be easily polished in the $HNO_3/HF/H_2O$ solution and the influences of different DRE processing times would be not obvious. If with H_2O_2 in this solution, the etching rate could be reduced, which enabled the well control of the DRE processes as shown in Fig. 4(C3), (C4) and (C5). The H_2O_2 has a higher oxidation capability than HNO_3, with the reaction scheme for H_2O_2 given as

$$2H\ {}_2O_2 + 4H^+ + Si \leftrightarrow 4H_2O + Si^{4+}$$

Silicon will be dissolved into the ionized state by H_2O_2, thus making oxidation by HNO_3 difficultly. Therefore, H_2O_2 slowed the rate of the oxidation reaction by interrupting the autocatalytic reaction of HNO_3, leading to a lower etching rate of the $HNO_3/HF/H_2O$ solution (Park et al., 1995). To demonstrate influences of different DRE processing times distinctly, H_2O_2 was added to the $HNO_3/HF/H_2O$ solution to do the DRE processes.

Reflectance curves for each sample were shown in Fig. 5, with the weighted average reflectance values given in Table 3. The weighted average reflectance value for C1 was 36.39% because of the conventional “worm-like” textures. After fabrication of black silicon without DRE processes, the weighted average reflectance value of the silicon wafer was only 3.82%. The data clearly showed that nanostructures could sharply reduce sample reflectivity. After DRE processes for different times for samples C3 to C5, even though the reflectance of each sample increases to various degrees, they remained lower than that of C1. Clearly, the reflectivity increased with increasing etching time. This behavior could be explained by two factors. Firstly, microstructures increased both the reflection count for the incident light and the path of the incident light, provided the wafer with greater opportunity to absorb light. Second, the feature size of the nanostructures were smaller than the wavelength of the incident light, with the surface essentially acted as an effective index medium that is optically flat. The observed decrease in the height of the nanohills led to a change in the gradient index for the effective index medium from $n_{air} = 1$ (refractivity of air) to $n_{Si} = 3.5$ (refractivity of silicon), which in turns led to increased reflectivity.

To study the influence of the DRE processing time on the effect of

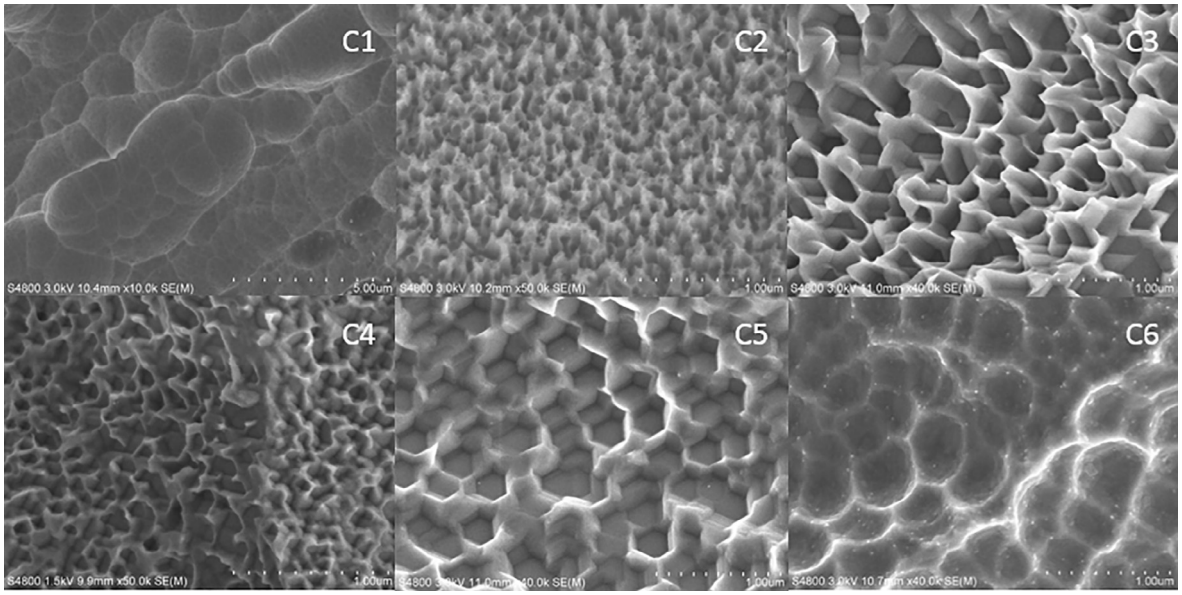

Fig. 4. SEM of images for a DWS mc-Si wafer surface processed under different conditions: C1: conventional acid-textured without black silicon; C2: black silicon without DRE process; C3: black silicon, $HNO_3/HF/H_2O_2/H_2O$ 1 min; C4: black silicon, $HNO_3/HF/H_2O_2/H_2O$ 3 min; C5: black silicon, $HNO_3/HF/H_2O_2/H_2O$ 6 min; C6: black silicon, HNO_3/HF /H_2O 1 min without H_2O_2.

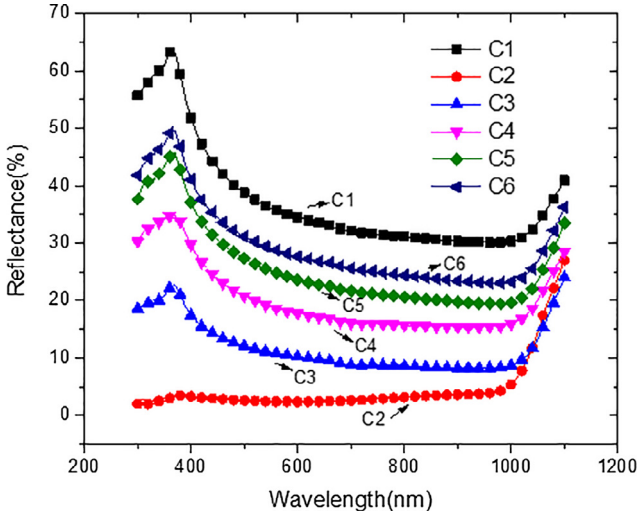

Fig. 5. Reflectance curves for DWS mc-Si wafers prepared under different conditions without SiN_x films.

Table 3
The weighted average reflectance values of DWS mc-Si wafers without a SiN_x films and DWS mc-Si solar cells prepared under different conditions.

	Weighted average reflectance values of samples without SiN_x films	Weighted average reflectance values of solar cells
C1	36.39%	13.99%
C2	3.82%	3.71%
C3	11.26%	5.60%
C4	19.46%	6.70%
C5	25.08%	9.08%
C6	28.92%	–

passivation, all samples were passivated by SiN_x on both faces after PSG removal, followed to measure the effective carrier lifetime (τ_{eff}) of minority carriers. Generally, the effective carrier lifetime (τ_{eff}) of minority carriers with a diffused emitter is expressed as

$$\frac{1}{\tau_{eff}} = \frac{1}{\tau_{bulk}} + \frac{(S_{eff}^{F} + S_{eff}^{B})}{d} \quad (2)$$

where τ_{bulk} is the bulk lifetime, S_{eff}^{F} and S_{eff}^{B} are the effective surface recombination velocities at the front and back surfaces, respectively, and d is the wafer thickness (Oh et al., 2012). In our experiments, the bulk lifetime τ_{bulk}, S_{eff}^{B} and d were almost the same for every wafer. Thus, effective surface recombination velocities S_{eff}^{F} could be characterized by τ_{eff}. The effective carrier lifetimes for the samples were given in Table 4. We could find that the effective carrier lifetime for C2 without the DRE processes is only 14.64 μs, which was far below other samples. It's proved that DRE processes is necessary for black silicon solar cells. Meanwhile, the effective carrier lifetime for C3, C4 and C5 increased in this order. Clearly, the effective carrier lifetime was influenced by the surface structures: the longer acidic DRE processes time, the longer lifetime. As we known, the τ_{eff} can be used to characterize the passivation effect, which influenced the IQE of the solar cell. the IQE of the solar cell. Thus, the results demonstrated that the surface structures of the wafer strongly influenced the passivation effect. The influences could be explained by two factors. Firstly, the wafer with the larger surface structure had a larger surface area; resulting in more recombination centers. Secondly, numerous sharp spikes were observed in the structures of C2 and C3, which would influence the passivation effect.

Fig. 6 showed the reflectance curves and the IQE and the EQE in relation to the wavelength and I-V curves of solar cells prepared using different DRE processes. The weighted average reflectance values for solar cells with SiN_x films for each sample were given in Table 3. The data clearly showed that the weighted average reflectance value of the

Table 4
The effective carrier lifetime for each wafer with passivation on both faces by SiN_x.

Sample	Effective carrier lifetime/μs
C1	62.01
C2	14.64
C3	43.60
C4	55.89
C5	58.06

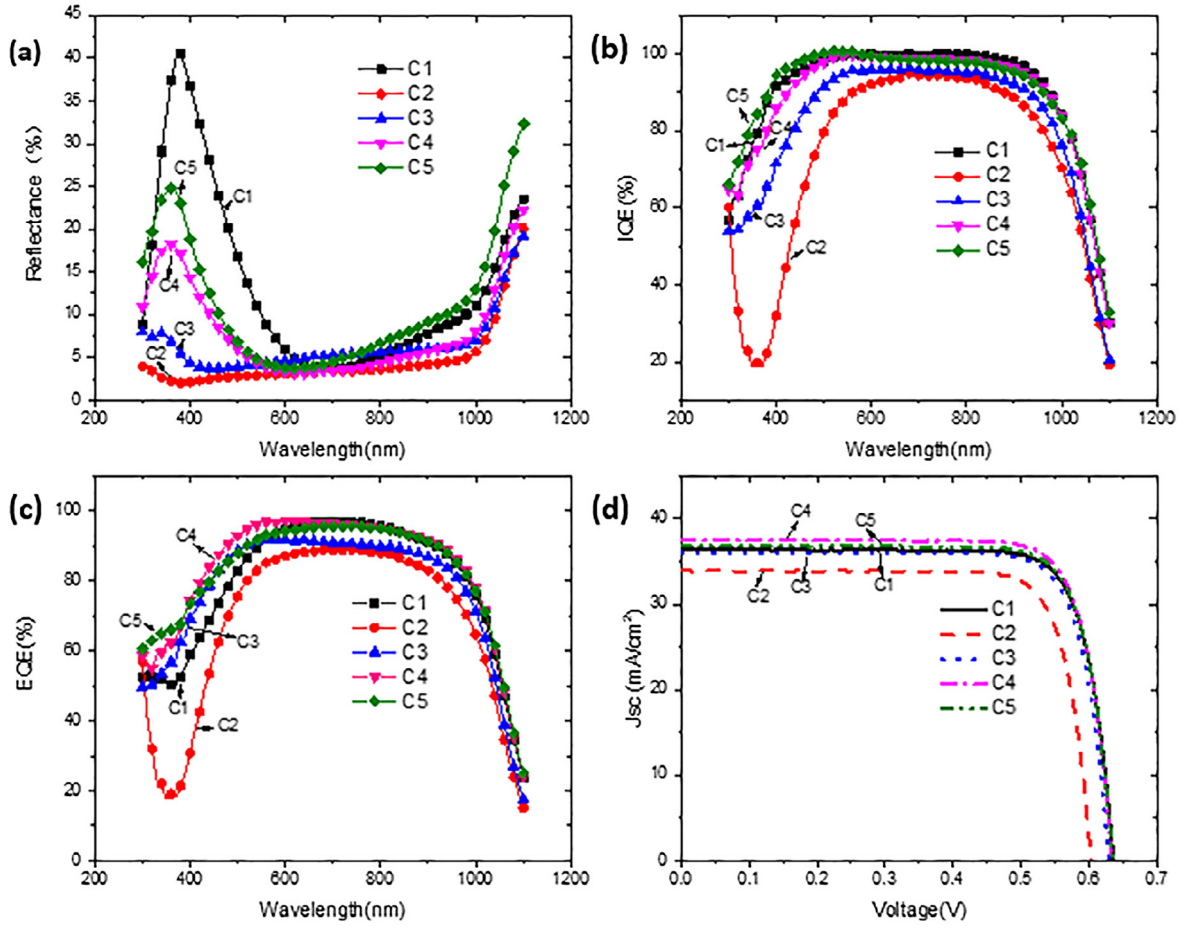

Fig. 6. (a) Reflectivity curves of DWS mc-Si solar cells under different conditions; (b) IQE curves of solar cells under different conditions; (c) EQE curves of solar cells under different conditions; and (d) I-V curves of solar cells under different conditions.

C1 solar cell was the highest (13.99%) and that of C2 solar cell was lowest (3.71%). Comparison of solar cells of C3, C4 and C5, the weighted average reflectance value of the solar cells increased with increasing etching time. Reflectance curves clearly showed that reflectances of samples were different in the wavelength range from 300 nm to 600 nm, with black silicon solar cells prepared using the DRE process absorbed more light in the wavelength range from 300 nm to 600 nm than the solar cell without black silicon (C1). Fig. 6(b) showed that the IQE of the solar cells (C3, C4 and C5) also increased with increased etching time. The results of effective carrier lifetime and the IQE indicated that the reflectivity shouldn't be as low as possible for black silicon solar cells: lower reflectivity needed larger surface area, which would lead to the poor passivation effect. For samples of C1, C4, C5 and C1, many differences were observed in the EQE curves in the wavelength range from 300 to 600 nm mainly because of differences in reflectivity in the same wavelength range. The EQE for C3 and C2 were lower in the wavelength range from 300 to 1100 nm mainly because of the poor passivation effect.

Fig. 7 showed the electroluminescence (EL) images for the solar cells prepared under different conditions. As we known, the EL intensity distribution clearly agreed well with the mapping of the minority carrier diffusion length in the sample because the EL intensity is proportional to the total excess minority carrier density (Fuyuki et al., 2005) (Fuyuki and Kitiyanan, 2009). The EL intensity is also proportional to the lifetime of the minority carriers. The EL image of C2 was the darkest among the sample images, which indicated that the minority carrier diffusion length of C2 relates to the structures distributed across the wafer surface. The EL images taken for samples C1, C3, C4 and C5 demonstrated that the wafer structure affects both the lifetime of minority carriers and the passivation effect. These results were consistent with the measured effective carrier lifetime (τ_{eff}) of the minority carriers.

Table 5 showed the main characteristics of the DWS mc-Si solar cells prepared under different conditions. The solar cell prepared under condition C4 showed the highest conversion efficiency (19.07%), followed by the cells prepared under conditions C5, C1, C3, and C2, in this sequence. The solar cell C4 showed the highest J_{sc} (37.55 mA/cm^2) under the common effect of its lower reflectivity than C5, C1 solar cells and better passivation effect than C2, C3 solar cells. The solar cell C2 showed the lowest reflectivity but also the lowest J_{sc} (33.95 mA/cm^2), even lower than that of C1 without black silicon (36.42 mA/cm^2). Meanwhile, the open-circuit voltage for C2 was the lowest (603 mV) because of the poor passivation effect. A comparison of C3, C4 and C5 revealed that the V_{oc} for C5 was the highest (635 mV) due to the effect of passivation. Although the reflectivity and the V_{oc} for C4 were neither the lowest nor the highest (634 mV), the J_{sc} and efficiency for C4 were the highest (37.55 mA/cm^2), which meant that the balance between reflectivity and recombination velocities was important for black silicon solar cell efficiency. For DWS black silicon solar cells, an extraordinary low reflectivity would result in a high recombination velocity and influence the passivation effect. These observations indicated that a suitable DRE process was necessary for black silicon solar cells, as demonstrated in other studies (Cao et al., 2015; Ye et al., 2015). Black silicon technique (MACE) with a suitable DRE process could improve the conversion efficiency of DWS silicon solar cells. This work showed a 0.6% improvement in efficiency compared to that of a traditional acid-textured DWS mc-Si solar cell.

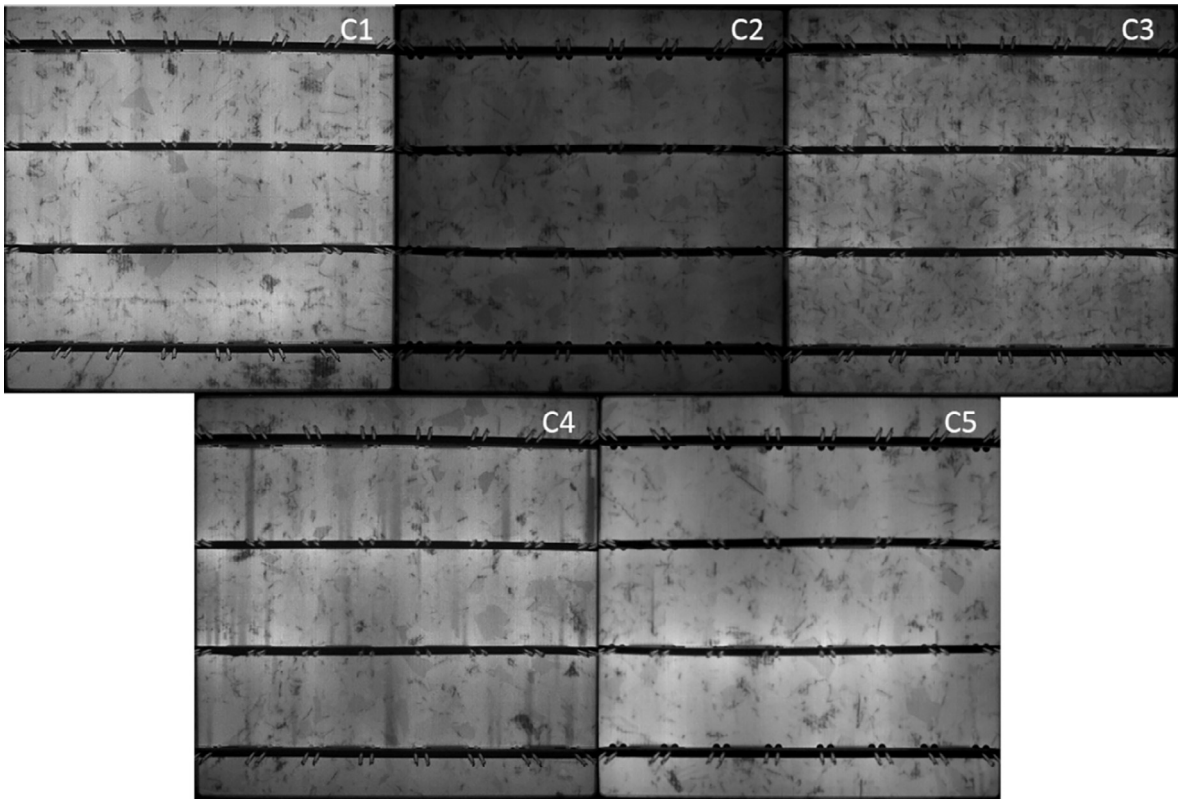

Fig. 7. EL images for DWS mc-Si solar cells prepared under different conditions.

Table 5
Performances of DWS mc-Si solar cells prepared under different conditions.

	V_{oc}/mV	J_{sc}/mA cm^{-2}	R_s/Ω	*FF*/%	Eff./%
C1	636	36.42	0.0020	79.75	18.47
C2	603	33.95	0.0016	78.78	15.98
C3	629	36.09	0.0020	79.18	17.99
C4	634	37.55	0.0018	80.07	19.07
C5	635	36.86	0.0019	80.09	18.75

4. Conclusions

In summary, a DWS mc-Si wafer was successfully textured by the MACE process. Subsequent DRE processing with different etching times was studied. The size of nanohills decreased and the reflectivity of DWS mc-Si wafers increased with increasing etching time. Wafers prepared under different DRE conditions together with a wafer without black silicon structures were used to fabricate solar cells. The IQE and performances of the cells showed that a balance keeping between reflectivity and recombination was important for the black silicon solar cells. The τ_{eff} measurement results and EL images of the solar cells strongly supported the above conclusions. The J_{sc} for a DWS mc-Si solar cell prepared by MACE and DRE processed could be improved to 37.55 mA/cm^2, with a best conversion efficiency of 19.07%, which showed an efficiency gain of 0.6%, as compared with the efficiency of a conventional acid-textured DWS mc-Si solar cell.

Acknowledgements

This work was supported by the National Natural Science Foundation of China (Grant Nos. 110751402347, 61274059, 51702355, 51602340).

References

Cao, F., Chen, K., Zhang, J., Ye, X., Li, J., Zou, S., Su, X., 2015. Next-generation multi-crystalline silicon solar cells: diamond-wire sawing, nano-texture and high efficiency. Sol. Energy Mater. Sol. Cells 141, 132–138.
Fuyuki, T., Havato, K., Yamazaki, T., Yu, T., Yukiharu, U., 2005. Photographic surveying of minority carrier diffusion length in polycrystalline solar cells by electro-luminescence. Appl. Phys. Lett. 86 (26), 262108–262108-3.
Fuyuki, T., Kitiyanan, A., 2009. Photographic diagnosis of crystalline silicon solar cells utilizing electroluminescence. Appl. Phys. A 96 (1), 189–196.
Holt, A., Thøgersen, A., Rohr, C., Bye, J.I., Helgesen, G., Nordseth, ø., Jensen, S.A., Norheim, l., Nielsen, ø., 2010. Surface structure of mono-crystalline silicon wafers produced by diamond wire sawing and by standard slurry sawing before and after etching in alkaline solutions. In: Photovoltaic Specialists Conference. pp. 12, 003501–003504.
Huang, Z., Geyer, N., Werner, P., De, B.J., Gosele, U., 2011. Metal-assisted chemical etching of silicon: a review. Adv. Mater. 23 (2), 285–308.
Huang, B., Zhao, J., Chai, J., Xue, B., Zhao, F., Wang, X., 2017. Environmental influence assessment of China's multi-crystalline silicon (multi-Si) photovoltaic modules considering recycling process. Sol. Energy 143, 132–141.
Jiang, Y., Shen, H., Pu, T., Zheng, C., Tang, Q., Gao, K., Wu, J., Rui, C., Li, Y., Liu, Y., 2017. High efficiency multi-crystalline silicon solar cell with inverted pyramid nanostructure. Sol. Energy 142, 91–96.
Koynov, S., Brandt, M.S., Stuttzmann, M., 2006. Black nonreflecting silicon surfaces for solar cells. Appl. Phys. Lett. 88, 203107.
Koynov, S., Brandt, M.S., Stuttzmann, M., 2007. Black multi-crystalline silicon solar cells. Phys. Status Solidi (RRL) 1, R53–R55.
Kim, C., Lee, J., Lim, S., Jeong, C., 2015. Enhanced absorption and short circuit current density of selective emitter solar cell using double textured structure. Sol. Energy 116, 265–271.
Kumagai, A., 2015. Texturization using metal catalyst wet chemical etching for multi-crystalline diamond wire sawn wafers. Sol. Energy Mater. Sol. Cells 133, 216–222.
Kim, M.H., Song, J.W., Nam, Y.H., Kim, D.H., Yu, S.Y., Moon, H.G., Yoo, B., Lee, J.H., 2016. Nanotexturing and post-etching for diamond wire sawn multicrystalline silicon solar cell. J. Korean Inst. Surf. Eng. 49 (3), 301–306.
Liu, X., Coxon, P.R., Peters, M., Hoex, B., Cole, J.M., Fray, D.J., 2014. Black silicon: fabrication methods, properties and solar energy applications. Energy Environ. Sci. 7 (10), 3223–3263.
Liu, T., Ge, P., Bi, W., Wang, P., 2017. Fracture strength of silicon wafers sawn by fixed diamond wire saw. Sol. Energy 157, 427–433.
Menna, P., Francia, G.D., Ferrara, V.L., 1995. Porous silicon in solar cells: a review and a description of its application as an AR coating. Sol. Energy Mater. Sol. Cells 37 (1), 13–24.
Meinel, B., Koschwitz, T., Acker, J., 2012. Textural development of SiC and diamond wire

sawed sc-silicon wafer. Energy Procedia 27 (7), 330–336.
Meinel, B., Koschwitz, T., Blocks, C., Acker, J., 2014. Comparison of diamond wire cut and silicon carbide slurry processed silicon wafer surfaces after acidic texturisation. Mater. Sci. Semicond. Proc. 26 (1), 93–100.
Niu, Y.C., Liu, H.T., Liu, X.J., Jiang, Y.S., Ren, X.K., Cai, P., Zhai, T.G., 2016. Study on nano-pores enlargement during Ag-assisted electroless etching of diamond wire sawn polycrystalline silicon wafers. Mater. Sci. Semicond. Proc. 56, 119–126.
Oh, J., Yuan, H.C., Branz, H.M., 2012. An 18.2%-efficient black-silicon solar cell achieved through control of carrier recombination in nanostructures. Nature Nanotechnol. 7 (11), 743.
Park, T.H., Ko, Y.S., Shim, T.E., Lee, J.G., 1995. The cleaning effects of HF-HNO_3-H_2O_2 system. J. Electrochem. Soc. 142, 571–572.
Park, K.M., Lee, M.B., Shin, J.W., Choi, S.Y., 2013. Investigation of surface features using reactive ion etching method for the enhanced performance of multi-crystalline silicon solar cells. Sol. Energy 91, 37–47.
Sopori, B., Devayajanam, S., Basnyat, P., Schnepf, R., Sahoo, S., Gee, J., Severico, F., Seigneur, H., Schoenfeld, W., Preece, S., Binns, J., Appel, J., Vansant, K., 2015. Surface damage introduced by diamond wire sawing of si wafers: measuring in-depth and the lateral distributions for different cutting parameters. MRS Proc. 1770, 61–66.
Wehrspohn, R., Sprafke, A.N., 2014. Black silicon photovoltaics. J. Opt. Soc. Am. B 3, 147–164.
Xiao, G., Liu, B., Liu, J., Xu, Z., 2014. The study of defect removal etching of black silicon for solar cells. Mater. Sci. Semicond. Proc. 22 (1), 64–68.
Xiao, Z., Geng, G., Wei, X., Yue, Z., Zhou, L., 2016. On the mechanism of the vapor etching of diamond wire sawn multi-crystalline silicon wafers for texturing. Mater. Sci. Semicond. Proc. 53, 8–12.
Yang, L., Liu, Y., Wang, Y., Chen, W., Chen, Q., Wu, J., Kuznetsov, A., Du, X., 2017. 18.87%-efficient inverted pyramid structured silicon solar cell by one-step Cu-assisted texturization technique. Sol. Energy Mater. Sol. Cells 166, 121–126.
Ye, X., Zou, S., Chen, K., Li, J., Huang, J., Cao, F., Wang, X., Zhang, L., Wang, X., Shen, M., Su, X., 2015. 18.45%-Efficient multi-crystalline silicon solar cells with novel nanoscale pseudo-pyramid texture. Adv. Funct. Mater. 24 (42), 6708–6716.
Yu, H.J.J., Popiolek, N., Geoffron, P., 2016. Solar photovoltaic energy policy and globalization: a multiperspective approach with case studies of Germany, Japan, and China. Prog. Photovolt. 24 (4), 458–476.
Yu, Z., Ma, W., Xie, K., Lv, G., Chen, Z., Wu, J., Yu, J., 2017. Life cycle assessment of grid-connected power generation from metallurgical route multi-crystalline silicon photovoltaic system in China. Appl. Energy 185, 68–81.